

# Configurable Beam-Steering Network for Phase Array Antennas- Part I: Proposed Configurable Photonic True Time Delay Line

Duaa Alyas Karim Aljaf<sup>1,\*</sup>, Raad Sami Fyath<sup>2</sup>

<sup>1</sup>Department of Electronic and Communications Engineering, Al-Nahrain University, Baghdad, Iraq

<sup>2</sup>Department of Computer Engineering, Al-Nahrain University, Baghdad, Iraq

---

**Abstract** Beam-steering networks for phase array antennas (PAAs) have been successfully and efficiently implemented in the literature using photonic true time delay line (TTDL). The delay line has been designed according to the operating microwave frequency  $f_{mw}$  and number of radiating elements  $N$  of the PAA and cannot be adopted efficiently for other PAAs operating at different parameters values. Future wireless communication base stations will deal with PAAs having different values of  $f_{mw}$  and  $N$  and therefore, it is essential to design smart beam-steering networks. In this paper, a configurable photonic TTDL is proposed for PAA beam-steering network. The delay line consists of cascaded linearly chirped fiber Bragg gratings (LCFBGs) whose number is adopted according to the operating frequency, number of radiating elements, and steering angle. A parametric study of the used LCFBG is performed and the simulation results reveal that a FBG designed with 80 mm length and modified Gaussian apodization offers a 562 ps time delay difference across its reflectively spectrum bandwidth (4 nm). The scanning capabilities of PAAs incorporating this configurable photonic delay line is investigated and the results are given in the accompanying paper [1]. The simulation results reported here are obtained using "OptiGrating ver. 14-1" Software.

**Keywords** Phase array antenna, Linearly chirped fiber Bragg grating, Microwave photonics, True time delay line

---

## 1. Introduction

Recently, there is increasing interest in microwave photonics (MWP)-based signal processing which connects microwave domain with optical domain [2, 3]. The MWP technique enables efficient generation and processing of microwave signals using photonic technology [4, 5]. The main inherent features of MWP are immunity to electromagnetic interference, low loss, wide-bandwidth operation, compactness, and light weight [6, 7]. Further, MWP can offer tunability and reconfigurability for the whole system, which is hard to realize using conventional microwave technologies [8, 9].

One of the main applications of MWP is beam steering and beam forming of microwave and millimeter wave phase array antennas (PAAs) [10, 5]. This application has been demonstrated successfully for wireless communications [11-13] and radar imaging systems [14]. The steering

operation of traditional PAAs relies on microwave phase shifters which are used to control the phase of each radiating elements (sub-antenna) in the PAA. The interference of electromagnetic waves from these radiating elements control the beam pattern in the free space. Microwave photonic phase shifters suffer from beam-squint problem which limits the operation bandwidth [5]. This problem arises due to the dependence of beam steering angle on the microwave frequency which leads to the divergence of beam directions of different microwave frequencies at increasing steering angles. This problem can be solved by using a true time delay line (TTDL) which offers a linear phase shift-frequency characteristics and hence ensures a frequency-independent steering angle. Photonic delay line has been emerged as promising candidates for TTDL beam steering networks in terms of loss and bandwidth beside its suitability for implementation in MWP platform [15, 16]. In photonic beam steering network, the microwave signal is mapped into an optical carrier. The modulated optical carrier is then launched into the photonic TTDL to get the required delay and the resultant optical signal is photodetector to get a delayed version of the microwave signal.

It is worth to mention here that photonic-based beam steering networks cannot be in general realized using

---

\* Corresponding author:

doaa.engeneering@gmail.com (Duaa Alyas Karim Aljaf)

Published online at <http://journal.sapub.org/ijnc>

Copyright © 2019 The Author(s). Published by Scientific & Academic Publishing

This work is licensed under the Creative Commons Attribution International

License (CC BY). <http://creativecommons.org/licenses/by/4.0/>

conventional photonic transmission lines (optical fibers or optical waveguides). These photonic lines offer time delay which is almost independent of the laser wavelength. The time delay  $\Delta\tau$  offered by photonic line of length  $\Delta L$  is given by  $\Delta\tau = n \Delta L/c$ , where  $c$  is the speed of light in free space and  $n$  is the refractive index of propagation medium. Therefore, the phase shift  $\Delta\phi$  between successive radiating elements cannot be varied by tuning the laser wavelength. In contrast, photonic TTDL implemented using fiber Bragg grating (FBG) technology offers a time delay  $\Delta\tau(\lambda)$  which is a function of the laser wavelength  $\lambda$  [6]. The corresponding phase shift  $\Delta\phi(\lambda) = 2\pi \Delta\tau(\lambda)/T_{mw} = 2\pi c \Delta\tau(\lambda)/\lambda_{mw}$  where  $T_{mw} = 1/f_{mw}$  is the time period of a microwave signal of frequency  $f_{mw}$  (or wavelength  $\lambda_{mw}$ ). Hence the steering angle  $\theta_s = \sin^{-1}(\lambda_{mw} \Delta\phi/2\pi d)$  [17] becomes equal to  $\sin^{-1}[c \Delta\tau(\lambda)/d]$ , where  $d$  is the radiating elements spacing. In this case  $\theta_s$  is independent of the microwave signal spectral contents and can be controlled by tuning the laser wavelength  $\lambda$ . The individual radiating elements are frequently spaced about a half-wavelength apart (i.e.,  $d = \lambda_{mw}/2$ ), where  $\lambda_{mw}$  is taken as the center wavelength of the microwave signal spectrum. This makes  $\theta_s = \sin^{-1}[2 f_{mw} \Delta\tau(\lambda)]$ . Therefore, to obtain a fixed value of  $\theta_s$ , the time delay  $\Delta\tau(\lambda)$  should be adapted according to the operating microwave frequency  $f_{mw}$ . At low microwave frequencies, the required value of  $\Delta\tau(\lambda)$  can not be obtained by one FBG and cascaded configuration of photonic TTDLs is required. This issue is addressed in this paper where an adaptive photonic TTDL is proposed using FBGs and optical switches. The concepts of this work may be applied in base stations of wireless communication systems which will deal with PAAs having different values of  $f_{mw}$  and number of radiating elements. Therefore, it is essential to design smart beam-steering networks for these base stations and this subject will be addressed in the accompanying paper [1].

## 2. Background on Apodized Linearly Chirped Fiber Bragg Grating

This section introduces the main concepts of FBG and its linearly chirped version. The principles of refractive index-apodization profiles are briefly illustrated.

### 2.1. Concepts of Fiber Bragg Grating

Fiber Bragg gratings (FBGs) are formed by constructing a periodic or a quasi-periodic modulation of refractive index inside the core of an optical fiber, see Figure 1. This change in index of refraction is typically created by exposing the fiber core to an intense interference pattern of UV energy. The exposure produces a permanent increase in the refractive index of the fiber's core, creating a fixed index modulation according to the exposure pattern. This fixed index modulation is called a grating [18]. A small amount of light is reflected at each period. All the reflected light

signals combine coherently to one large reflection at a particular wavelength. This is referred to as the Bragg condition, and the wavelength at which this reflection occurs is called the Bragg wavelength. Only those wavelengths that satisfy the Bragg condition are affected and strongly back reflected through the same core of the fiber. Uniform FBGs are based on a periodical modulation of the refractive index in the core of an optical fiber Figure 1, and they are the most popular grating-based type of technology.

The Bragg wavelength  $\lambda_B$  equals to [19]

$$\lambda_B = 2\Lambda n_{eff} \quad (1)$$

where  $\Lambda$  is the period of the refractive index modulation, and  $n_{eff}$  is the effective refractive index of the fiber core. In a chirped FBG, periodicity of the modulation is not constant, but it changes along the propagation axis  $z$ ; the function  $\Lambda(z)$  defines the chirp pattern. This implies that each different section of the grating reflects a different Bragg wavelength, and the overall spectrum of the FBG results from the spectrum of each section of the grating.

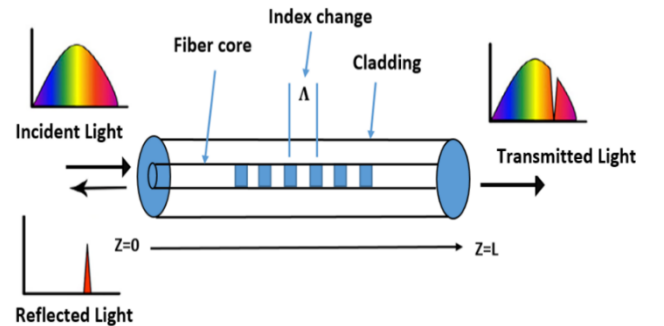


**Figure 1.** Concept of fiber Bragg grating. Illustrative spectra of the incident, reflected and transmitted waves are given

Consider an uniform FBG extended along the  $z$ -axis from  $z=0$  to  $z=L$ . Assume that the periodic variation of the refractive index over the grating axial direction ( $z$ -axis) takes the following form [20]

$$n(z) = n_0 + \Delta n \sin(2\pi z/\Lambda) \quad (2)$$

where  $n_0$  is the axial average of the refractive index,  $\Delta n$  represents the peak of the refractive index variation, and  $\Lambda$  denotes the grating pitch which represents the period of the  $z$ -dependent refractive index variation as shown in Figure 2. The typical value of  $\Delta n$  varies in the range  $10^{-5}$  to  $10^{-2}$ . Under weak coupling (i.e.,  $\Delta n < n_0$ ), the fundamental mode of the grating wavelength can be expressed as [18]

$$E(z) = A(z)e^{-j\beta z} + B(z)e^{j\beta z} \quad (3)$$

where  $A(z)$  and  $B(z)$  represent forward- and backward-propagating modes, respectively, and  $\beta_p$  is the propagation constant

$$\beta_p = \frac{2\pi n_{eff}}{\lambda_0} \quad (4)$$

Here  $n_{eff}$  is the effective refractive index of the fundamental mode whose wavelength is  $\lambda_0$ .

The relation between the forward mode  $A(z)$  and the backward mode  $B(z)$  is governed by the following coupled equations [18]

$$\frac{dA}{dz} = k B(z) e^{i\Gamma z} \quad (5a)$$

$$\frac{dB}{dz} = k A(z) e^{-i\Gamma z} \quad (5b)$$

where  $k$  is the coupling coefficient

$$k = \frac{\pi \Delta n}{\lambda_o} \quad (5c)$$

$$\Gamma = 2\beta_p - 2\pi/\Lambda \quad (5d)$$

Equations 5a and 5b should be solved as two simultaneous equations to yield  $A(z)$  and  $B(z)$ . Taking the derivative of both sides of equ. 3 with respect to  $z$  yields

$$\frac{d^2 B}{dz^2} = k A(z) (-i\Gamma e^{-i\Gamma z}) + k \frac{dA}{dz} e^{-i\Gamma z} \quad (6a)$$

Substituting equ. 5a into equ. 6a gives

$$\frac{d^2 B}{dz^2} = -i\Gamma B(z) + k^2 B(z) \quad (6b)$$

$$\frac{d^2 B}{dz^2} + i\Gamma B(z) - k^2 B(z) = 0 \quad (7)$$

The solution that will incorporate the boundary condition ( $B(L) = 0$ )

$$B(z) = F e^{-(i/2)\Gamma z} \sinh \alpha(z - L) \quad (8)$$

where  $\alpha = \sqrt{k^2 - \frac{1}{4}\Gamma^2}$ .

Using equ. 5b yields

$$A(z) = \frac{F}{k} e^{(i/2)\Gamma z} \left[ -i\frac{\Gamma}{2} \sinh(z - L) + \alpha \cosh \alpha(z - L) \right] \quad (9)$$

Using the boundary condition  $A(0) = 1$  gives

$$F = \frac{k}{\alpha \cosh \alpha L + i\frac{\Gamma}{2} \sinh \alpha L} \quad (10)$$

The amplitude reflection coefficient is given by

$$r \equiv \frac{B(0)}{A(0)} = F \sinh(-\alpha L) \quad (11)$$

$$r = -\frac{k \sinh(\alpha L)}{\alpha \cosh \alpha L + i\frac{\Gamma}{2} \sinh \alpha L} \quad (12)$$

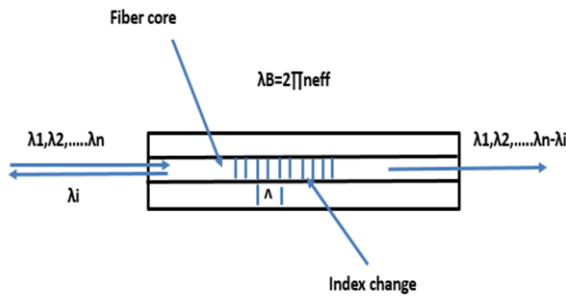


Figure 2. Refractive index change in optical fiber

## 2.2. Linearly Chirped FBG

The chirped FBG has nonuniform grating period  $\Lambda$  along its length  $z$ . When  $\Lambda(z)$  varies linearly with  $z$ , the structure is called linearly chirped (LC) FBG. The LCFBG is characterized by a wider reflection spectrum since each

wavelength component is reflected at different grating position. This type of FBG can be fabricated by varying the peak refractive index variation  $\Delta n$  (see equ. 2) with the axial length  $z$ . For an FBG extending from  $z = 0$  to  $z = L$ , the linearly chirped period can be expressed as [20]

$$\Lambda(z) = \Lambda_o + C_c \left(\frac{L}{2} - z\right) \quad (13a)$$

where  $\Lambda_o$  is the center period of the grating and  $C_c$  is the chirp parameter. The maximum and minimum grating periods occur at  $z = 0$  and  $z = L$ , respectively

$$\Lambda_{max} = \Lambda_o + C_c L/2 \quad (13b)$$

$$\Lambda_{min} = \Lambda_o - C_c L/2 \quad (13c)$$

Note that  $C_c = (\Lambda_{max} - \Lambda_{min})/L$  and  $\Lambda_{max} - \Lambda_{min}$  is the total chirp. Recall that the Bragg wavelength  $\lambda_B$  is related to the grating period  $\Lambda$  and effective refractive index  $n_{eff}$  by  $\lambda_B = 2n_{eff}\Lambda$ . Then for a LCFBG, the minimum and maximum value of the Bragg wavelength can be computed from

$$(\lambda_B)_{min} = 2n_{eff} \Lambda_{min} \quad (14)$$

$$(\lambda_B)_{max} = 2n_{eff} \Lambda_{max} \quad (15)$$

The dispersion parameter  $\beta$  of the FBG is defined as the variation of the time delay  $\tau$  associated with reflection transfer function with wavelength

$$\beta = d\tau/d\lambda \quad (16)$$

For a LCFBG, the dispersion parameter can be calculated approximately by

$$\beta_{LCFBG} = \frac{L/c}{(\lambda_B)_{max} - (\lambda_B)_{min}} = \frac{n_{eff} L/c}{2n_{eff}(\Lambda_{max} - \Lambda_{min})} = \frac{L}{4c\Lambda_o} \quad (17)$$

where  $\Lambda_o = (\Lambda_{max} - \Lambda_{min})/2$  which corresponds to the grating period at the axial center of the FBG. Note that  $\beta_{LCFBG}$  is constant over the spectral range of interest and this ensures a linear variation of time delay with  $\lambda$ . This feature is very important to design TTDL where the time delay can be varied linearly with the laser wavelength.

## 2.3. Apodization Profiles

Refractive index-apodization profile refers to the case when the peak of the refractive index variation  $\Delta n$  is not uniform along the FBG axis (see equ. 2). In this case  $\Delta n$  is  $z$ -dependent and can be expressed as

$$\Delta n(z) = (\Delta n)_u T(z) \quad (18)$$

where  $(\Delta n)_u$  corresponds to the uniform apodization profile where the peak of the refractive index is uniform across the length of the FBG and  $T(z)$  is the apodization profile or function. Note that  $T(z)$  is similar to a spatial window used in signal processing.

It is well known from the literature that using apodization and linear chirping in Bragg gratings reduces the side lobe level in the reflectivity response and also the group time delay response ripple [21]. However, different apodization profiles having different impact and it would be useful to choose the profile that is more suitable for the problem under investigation. In this work, the apodization profile is chosen to give large time delay difference across the LCFBG

spectrum. The investigation done in this work reveals that the best results are obtained by using two types of apodization profiles

- (i) Modified Gaussian Apodization (MGA) [22]

$$T(z) = \exp \left[ - \left[ \frac{2(z - \frac{L}{2})}{sL} \right]^n \right] \quad (19)$$

where  $n$  is the order of MGA and  $s$  is the taper parameter.

- (ii) Gaussian Apodization (GA) [22]

$$T(z) = \exp \left[ - \ln 2 \left[ \frac{2(z - \frac{L}{2})}{sL} \right]^2 \right] \quad (20)$$

Note that the two profiles are symmetric around the center of the grating and normalized such that  $|T(z)| \leq 1$ .

### 3. Proposed Beam-steering Network

#### 3.1. System Configuration

Figure 3 illustrates the main concepts of the configurable photonic TTDL-based beam-steering network investigated in this work. For  $N$ -element PAA, the outputs of  $N$ -tunable semiconductor lasers (TSLs) are multiplexed and the resultant waveform is then modulated by the microwave signal. The modulated multiplexed signal is launched into the configurable TTDL and the output is applied to 1: $N$  demultiplexer. Each of the demultiplexer output is detected by a photodiode (PD) to recover a delayed version of the microwave signal which is then amplified by a low-noise amplifier (LNA) before feeding the radiating element. The configurable photonic delay line consists of  $K$  cascaded identical FBGs. Successive FBGs are separated by electrically controlled optical switch (OS) (see Figure 3(b-d)). The OS operates in either bar state or cross state depending whether the state of the control signal is ON or OFF, respectively. When the OS operates in the bar state, the switch passes the input optical signal to next FBG for extra delay. In the cross state, the input signal does not need extra time delay and therefore passes directly to the demultiplexer input.

Few remarks related to the configurable photonic delay line are given in the following

- (i) The proposed TTDL is quite general and can be used with different PAAs having their own operating microwave frequencies and number of radiating elements.
- (ii) The first FBG is always in operation independent of the states of the OSs.
- (iii) The FBGs operate in the reflection mode. Therefore, the reflection transfer functions of the FBGs are used to determine the associated time delays.
- (iv) The proposed configurable delay line can be redesigned to use the transmission functions of the FBGs.

- (v) Nonidentical FBGs can be used to design the photonic line if needed for certain applications.

#### 3.2. Design Guidelines

The performance of the photonic TTDL depends mainly on the reflection characteristics of the employed FBGs. The design of the FBG should satisfy the following requirements

- (i) High-peak and wideband optical power reflection spectrum centered at a given wavelength  $\lambda_c$ . The wavelength of the used TSLs should distributed around the center wavelength  $\lambda_c$  and see almost the same power reflection. According to that, -0.5dB bandwidth measure is used here to estimate the bandwidth of the power reflection spectrum ( $B_\lambda$ ). This ensures 0dB (i.e., 100%) power reflection at the center wavelengths  $\lambda_c$  and -0.5dB (i.e., 89%) at the lower and higher cutoff wavelengths. The slight variations in the power reflections seen by the semiconductor lasers can be equalized at the receiver end by adapting the gains of the LNAs.
- (ii) Linear variation of the time delay associated with FBG amplitude (field) reflection transfer function across the spectrum and without ripple. This is useful to ensure a linear variation of the time delay with TSLs wavelength spacing.
- (iii) Large time delay across the spectrum  $\tau_d$  and it is preferred to yield high dispersion parameter  $\beta \equiv \tau_d / B_\lambda$ .

A linearly chirped FBG (LCFBG) is used in this delay line to yield a linear time delay-wavelength characteristics. The Bragg wavelength varies linearly along the FBG axis and yields a time delay that decreases linearly with the wavelength in the reflection spectrum bandwidth. Figure 4 shows an ideal time delay characteristics  $\tau(\lambda)$  of a LCFBG across the power reflection bandwidth  $B_\lambda = \lambda_{max} - \lambda_{min}$ . Here  $\lambda_{max}$  and  $\lambda_{min}$  are, respectively, the upper and low cutoff wavelengths of the spectrum. The chirp parameter of the FBG is a positive quantity and computed from

$$\beta \equiv \frac{\tau_d}{B_\lambda} = \frac{\tau(\lambda_{min}) - \tau(\lambda_{max})}{\lambda_{max} - \lambda_{min}} \quad (21)$$

The time delay at a given wavelength  $\lambda_i$  within the reflection bandwidth can be expressed as

$$\tau_i = \tau_r - \beta(\lambda_i - \lambda_r) \quad (22)$$

where  $\tau_i \equiv \tau(\lambda_i)$  and  $\tau_r \equiv \tau(\lambda_r)$  are the time delays associated with  $\lambda_i$  and the reference wavelength  $\lambda_r$ , respectively.

The time delay difference between two adjacent TSLs whose wavelengths differs by  $\Delta\lambda$  is given by

$$\Delta\tau = \beta \Delta\lambda \quad (23)$$

where  $\Delta\lambda = \lambda_i - \lambda_{i-1}$  with  $\lambda_i > \lambda_{i-1}$ .

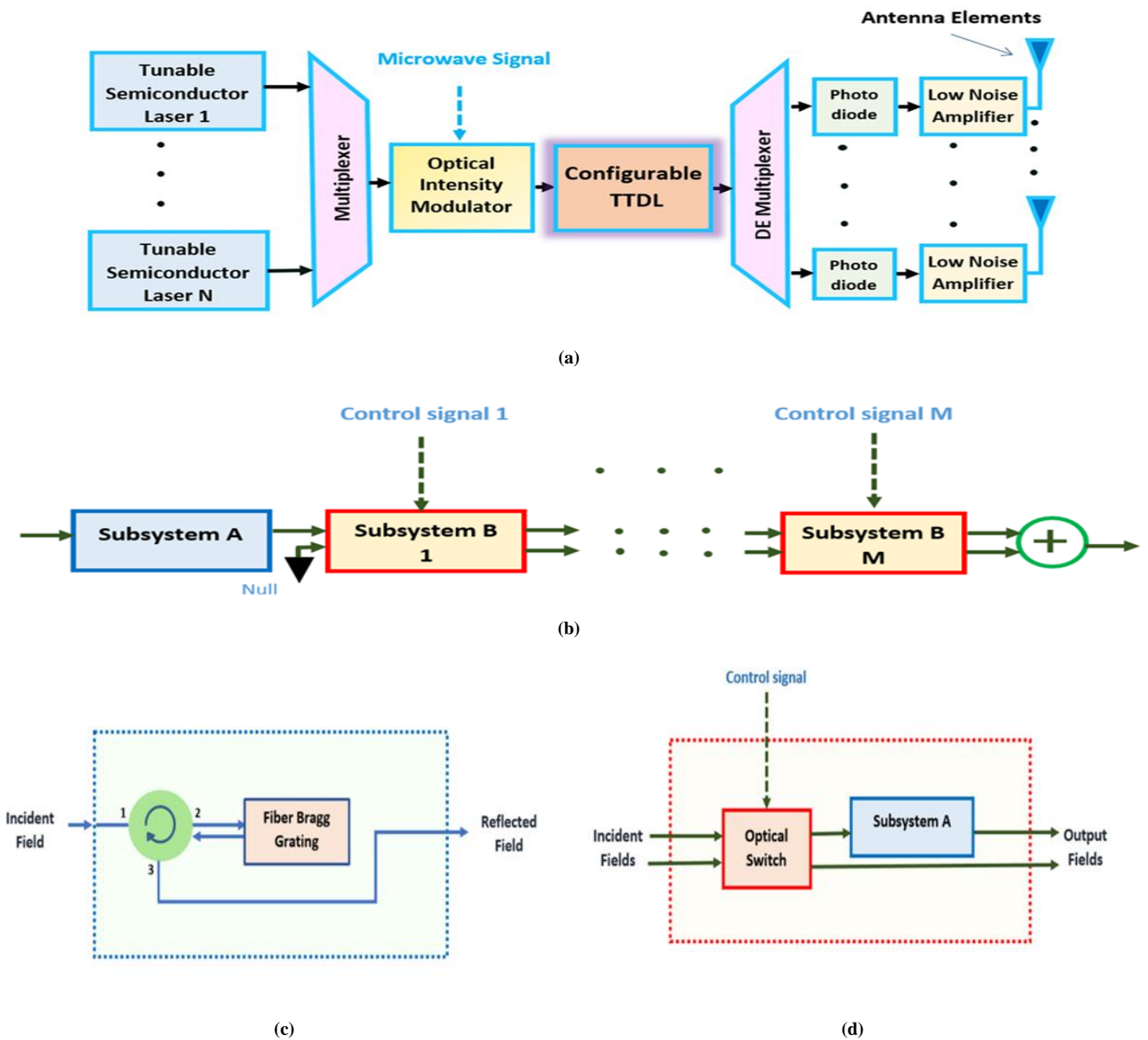


**Figure 3.** Proposed photonic TTDL-based beam steering. (a) System configuration; (b) Configurable photonic delay line; (c) Subsystem A; (d) Subsystem B

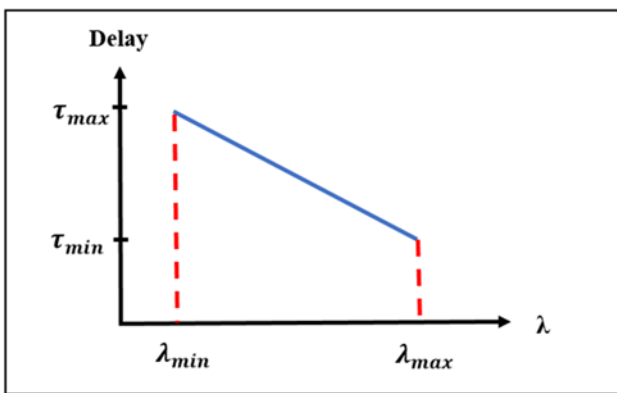


**Figure 4.** Time delay characteristics  $\tau(\lambda)$  of a LCFBG across the power reflection bandwidth

The TSLs operate in continuous-wave (CW) mode with equal wavelength spacing  $\Delta\lambda$ . The wavelengths of the TSLs ( $\lambda_i, i = 1, 2, \dots, N$ ) are assumed to be distributed symmetrically around the spectrum center wavelength. Figure 5 illustrates the wavelengths corresponding to a 4-element PAA.

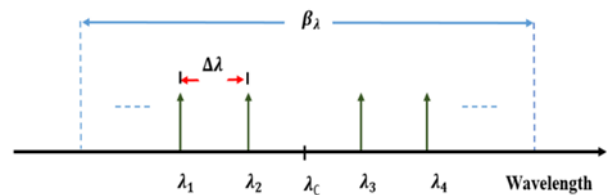


**Figure 5.** Wavelengths distribution of four TSLs used in the 4-element of PAA

When the PAA is designed with  $N$  even, the wavelengths of the unmodulated (CW) tunable lasers can be calculated using the following formula

$$\lambda_i = \lambda_c - \frac{(N+1-2i)}{2} \Delta\lambda \quad i = 1, 2, \dots, N \quad (24)$$

According to equ. (24),  $\lambda_1 = \lambda_c - (N-1) \Delta\lambda/2$  and  $\lambda_N = \lambda_c - (N-1) \Delta\lambda/2$ .

The maximum wavelength spacing  $(\Delta\lambda)_{max}$  is set to  $B_\lambda/N$  to ensure that the wavelengths of the first and last lasers (i.e.,  $\lambda_1$  and  $\lambda_N$ ) are not located at the spectrum edges. According to that  $\lambda_1 > \lambda_{min}$  and  $\lambda_N < \lambda_{max}$  even when  $\Delta\lambda$  approaches its maximum value. Setting  $(\Delta\lambda)_{max}$  to  $B_\lambda/N$  is useful to tolerate FBG fabrication error. In other words, this setting ensures that the wavelengths of the TSLs are laying within the FBG spectrum. When  $\Delta\lambda$  tends to its maximum value  $(\Delta\lambda)_{max}$ , then  $\lambda_1$  and  $\lambda_N$  approach their minimum and maximum values, respectively.

$$(\lambda_1)_{min} = \lambda_c - \frac{(N-1)}{2N} B_\lambda \quad (25a)$$

$$(\lambda_N)_{max} = \lambda_c + \frac{(N-1)}{2N} B_\lambda \quad (25b)$$

Additional design guidelines related to single- and multi-FBG steering networks along with the used OS are given in the following subsections.

#### a- Single-FBG Steering Network

Consider now a uniform linear PAA having  $N$  radiating elements and operates with a microwave frequency  $f_{mw}$  with its beam-steering network uses a single LCFBG. The phase shift  $\Delta\phi$  between two successive radiating elements is related to the corresponding time delay difference by

$$\Delta\phi = 2\pi \Delta\tau/T_{mw} = 2\pi f_{mw} \Delta\tau = 2\pi f_{mw} \beta \Delta\lambda \quad (26)$$

where  $T_{mw}$  and  $f_{mw}$  is the period and frequency of the microwave signal used to modulate the lasers optical carriers, respectively. Then the steering angle  $\theta_s$  is given by

$$\begin{aligned} \theta_s &= \sin^{-1}(\lambda_{mw} \Delta\phi/2\pi d) = \sin^{-1}(c \Delta\tau/d) \\ &= \sin^{-1}(c\beta \Delta\lambda/d) \end{aligned} \quad (27)$$

The argument of the  $\sin^{-1}$  function should not exceed 1. This yields the following threshold condition which determines the upper bound of the wavelength spacing,  $(\Delta\lambda)_u$

$$(\Delta\lambda)_u = d/c\beta \leq (\Delta\lambda)_{max} = B_\lambda/N \quad (28)$$

If the network operates with  $\Delta\lambda = (\Delta\lambda)_{max}$ , then the maximum achievable steering angle is given by

$$(\theta_s)_{max} \equiv \theta_s|_{(\Delta\lambda)_{max}} = \sin^{-1}(c\beta B_\lambda/Nd) \quad (29)$$

According to equ. (29), the maximum number of radiating elements of the antenna whose beam can be steered toward  $90^\circ$  using one FBG-based network is computed from

$$N_{max} = \lfloor c\beta \lambda_B/d \rfloor \quad (30a)$$

$$= \lfloor 2f_{mw} \beta B_\lambda \rfloor \quad \text{when } d = \lambda_{mw}/2 \quad (30b)$$

where  $\lfloor \cdot \rfloor$  denotes the maximum integer in the argument.

#### b- Multi FBG-Based Beam-Steering Network

Consider the case when the beam steering is achieved by using number of FBGs,  $K_{FBG}$ , from the  $K$  cascaded FBG

available in the photonic line. The used optical circulators isolate the incident field from the reflected field for each used FBG. Therefore, the isolator acts as a buffer stage between two successive FBGs. Hence the total reflection transfer function of the  $K_{FBG}$  cascaded gratings can be computed as the product of the transfer functions of  $K_{FBG}$  gratings. The word ‘‘isolated’’ is used here to identify that the reflected field of the FBG does not affect the operation of the previous FBG in the cascaded network. According to this discussion, the total reflection transfer function of the  $K_{FBG}$  cascaded gratings can be expressed as

$$H_{tot}(f) = \prod_{k=1}^{K_{FBG}} H_{rk}(f) = |H_{tot}(f)| e^{j\theta_{tot}(f)} \quad (31a)$$

where  $H_{rk}(f)$  is the field reflection transfer function of the  $k$ th FBG involves in the operation and  $f$  is the optical frequency. Further, the magnitude and the phase of the total field reflection transfer function are expressed, respectively as

$$|H_{tot}(f)| = \prod_{k=1}^{K_{FBG}} |H_{rk}(f)| \quad (31b)$$

$$\theta_{tot}(f) = \sum_{k=1}^{K_{FBG}} \theta_{rk}(f) \quad (31c)$$

The total time delay  $\tau_{tot}$  seen by used cascaded FBGs is computed as

$$\begin{aligned} \tau_{tot}(f) &= \frac{1}{2\pi} \frac{d\theta_{tot}(f)}{df} = \frac{1}{2\pi} \sum_{k=1}^{K_{FBG}} \frac{d\theta_{rk}(f)}{df} \\ &= \sum_{k=1}^{K_{FBG}} (\tau_{FBG}(f))_k \end{aligned} \quad (32)$$

where  $(\tau_{FBG}(f))_k$  represents the time delay associated with the reflection transfer function of the  $k$ th FBG evaluated at the optical frequency  $f$ . Note that

- (i) The total time delay is the accumulation of the individual time delays of the used FBGs calculated under isolation condition.
- (ii) When the used FBGs are identical, then  $|H_{tot}(f)| = [|H_r(f)|]^{K_{FBG}}$  and  $\tau_{tot}(f) = K_{FBG} \tau_{FBG}$  where  $H_r$  and  $\tau_{FBG}$  correspond to a single FBG.
- (iii) If each FBG is designed to have 100% power reflection at the center frequency and -0.5dB bandwidth consideration, then the total power reflection evaluated at the FBG spectrum edges is 89.%, 79.4%, 70.8%, and 63.1% when  $K_{FBG} = 1, 2, 3,$  and  $4,$  respectively. This requires careful consideration to adapt the gains of the LNAs to compensate for the power reflection variation seen by the TSLs.
- (iv) For identical  $K_{FBG}$  gratings, the steering angle becomes

$$\theta_s = \sin^{-1}(K_{FBG} c\beta \Delta\lambda/d) \quad (33a)$$

$$(\theta_s)_{max} = \sin^{-1}(K_{FBG} c\beta \Delta\lambda/Nd) \quad (33b)$$

Then the minimum number of cascaded FBGs required to achieve maximum steering of  $90^\circ$  angle can be computed from

$$(K_{FBG})_{min} = \lceil Nd/c\beta B_\lambda \rceil \quad (33c)$$

$$= \lceil N/2f_{mw} \beta B_\lambda \rceil \quad \text{when } d = \lambda_{mw}/2 \quad (33d)$$

where  $\lceil \cdot \rceil$  denotes ceil function which rounds up the

argument to the next integer.

(v) Using element spacing  $d$  equals  $\lambda_{mw}/2$  yields

$$\theta_s|_{d=\lambda_{mw}/2} = \sin^{-1}(2K_{FBG} f_{mw} \beta \Delta\lambda) \quad (34a)$$

$$(\theta_s)_{max}|_{d=\lambda_{mw}/2} = \sin^{-1}(2K_{FBG} f_{mw} \beta B_\lambda/N) \quad (34b)$$

To achieve  $\theta_s = 90^\circ$ , the required wavelength difference  $\Delta\lambda$  can be estimated the following expression

$$\Delta\lambda|_{\theta_s=90^\circ} = 1/2\pi K_{FBG} f_{mw} \beta \quad (35a)$$

$$\text{and should be less than } B_\lambda/N. \quad (35b)$$

### c- 2×2 Optical Switch

The  $2 \times 2$  optical switch can be designed using Mach-Zehnder (MZ) configuration and implemented using silicon photonic platform. Figure 6 shows a schematic of MZ switch which consists of an input optical coupler, interferometric MZ region, and an output optical coupler. The control voltage is applied across one of the MZ arms to change its refractive index and hence introducing propagation phase difference with respect to the other arm [23].



**Figure 6.** Schematic of the  $2 \times 2$  Mach-Zehnder switch used in the proposed photonic delay line

The two electric fields at the optical coupler output are related to the two input fields by the following transfer matrix [24]

$$\mathbf{M}_c = \begin{bmatrix} a & jb \\ jb & a \end{bmatrix} \quad (36)$$

where  $a$  and  $b$  are, respectively, the bar and cross transmission coefficients of the coupler. The MZ interferometer (MZI) is assumed to have lossless arm waveguides and therefore, the transfer matrix  $\mathbf{M}_{MZ}$  which relates the output fields to the input fields will be determined by the propagation phases of the two arms

$$\mathbf{M}_z = \begin{bmatrix} e^{-j\phi_1} & 0 \\ 0 & e^{-j\phi_2} \end{bmatrix} \quad (37)$$

where  $\phi_1$  and  $\phi_2$  are, respectively, the phases gained by the electric fields at the end of the upper and lower waveguides.

If one assumes identical input and output couplers, the switch output fields  $E_3$  and  $E_4$  are related to its input fields  $E_1$  and  $E_2$  by

$$\begin{bmatrix} E_3 \\ E_4 \end{bmatrix} = \mathbf{M}_s \begin{bmatrix} E_1 \\ E_2 \end{bmatrix} \quad (38a)$$

where  $\mathbf{M}_s$  is the transfer function of the  $2 \times 2$  switch

$$\mathbf{M}_s = \mathbf{M}_c \mathbf{M}_{MZ} \mathbf{M}_c \quad (38b)$$

$$\mathbf{M}_s \equiv \begin{bmatrix} m_{11} & m_{12} \\ m_{21} & m_{32} \end{bmatrix} \quad (38c)$$

Using equs. (36) and (37) into equ. (38b) yields

$$m_{11} = a^2 e^{-j\phi_1} - b^2 e^{-j\phi_2} \quad (39a)$$

$$m_{12} = m_{21} = jab [e^{-j\phi_1} + e^{-j\phi_2}] \quad (39b)$$

$$m_{22} = -b^2 e^{-j\phi_1} + a^2 e^{-j\phi_2} \quad (39c)$$

Consider the practical case of  $a = b$  which corresponds to a 3dB-directional coupler. Introducing  $\phi_a = (\phi_1 + \phi_2)/2$  and  $\phi_d = (\phi_1 - \phi_2)$  as the phase average and difference, respectively, leads to

$$\begin{aligned} m_{11} &= a^2 e^{-j\phi_a} [e^{-j\phi_d/2} - e^{j\phi_d/2}] \\ &= -2ja^2 e^{-j\phi_a} \sin(\phi_d/2) \end{aligned} \quad (40a)$$

$$\begin{aligned} m_{12} = m_{21} &= ja^2 e^{-j\phi_a} [e^{-j\phi_d/2} + e^{j\phi_d/2}] \\ &= 2ja^2 e^{-j\phi_a} \cos(\phi_d/2) \end{aligned} \quad (40b)$$

$$\begin{aligned} m_{22} &= -a^2 e^{-j\phi_a} [-e^{-j\phi_d} + e^{j\phi_d/2}] \\ &= -2ja^2 e^{-j\phi_a} \sin(\phi_d/2) \end{aligned} \quad (40c)$$

Note that the condition  $a = b$  leads to  $m_{11} = m_{22}$ . Recall that  $m_{12} = m_{21}$  and this is independent of the condition  $a = b$ . Consider now the following special operating states

(i) Case I: No applied voltage

In this case,  $\phi_d = 0$  (assuming equal-length MZ arms). Then  $m_{11} = m_{22} = 0$  and  $m_{12} = m_{21} = j2a^2 e^{-j\phi_a}$ . This corresponds to cross-state operation. Since the optical power is proportional to the absolute-value square of the electric field, then  $P_3 = 4a^2 P_2$  and  $P_4 = 4a^2 P_1$ .

(ii) Case II: Voltage is applied to yield  $\phi_d = 180^\circ$

In this case  $m_{12} = m_{21} = 0$  and  $m_{11} = m_{22} = -j2a^2 e^{-j\phi_a}$ .

This indicates bar-state operation which yields  $P_3 = 4a^2 P_1$  and  $P_4 = 4a^2 P_2$ . The insertion loss of the switch,  $\alpha_{IL}$ , can be compared from

$$\alpha_{IL} = \frac{\text{Total Input power}}{\text{Total output power}} = \frac{P_1 + P_2}{P_3 + P_4}$$

For the two special cases mentioned above,  $\alpha_{IL} = 1/4a^2$ . Note that the loss of the directional coupler  $\alpha_c = 1/(a^2 + b^2)$  and this equals  $1/2a^2$  when  $a = b$ . For lossless coupler (i.e.,  $\alpha_c = 1$ ) then  $a = 1/\sqrt{2}$ . For lossy coupler,  $\alpha_c^2 > 1/2$ . Note further that  $\alpha_{IL} = 2 \alpha_c$  since the MZ waveguide arms are assumed lossless.

## 4. Performance Evaluation of Linearly Chirped FBG

The time delay-wavelength characteristics of the proposed photonic delay line depends on the reflection response of the used LCFBG. This section presents parametric study to characterize the time delay spectrum associated with the reflection transfer function of LCFBG operating with apodization profile and 1550 nm reference wavelength. The simulation results are obtained using the commercial software package "OptiGrating ver. 14-1". Initial simulation tests are performed to select the apodization profile suitable for efficient design of photonic.

TTDL-based beam steering. The target is to get

- (i) Large time delay difference across the FBG spectrum bandwidth (which is denoted here by  $\tau_d$ ).
- (ii) The time delay  $\tau(\lambda)$  varies linearly across the spectrum bandwidth without ripple.

The initial simulation tests performed in this work have shown that modified Gaussian apodization (MGA) designed with,  $n = 4$  and  $s = 0.7$  offers the best time delay spectrum performance. The next apodization profile to be used is the Gaussian (GA) designed with  $s = 0.5$ . Therefore, the investigation in this section focuses only on these two apodization types. In the following, results are reported for MGZ-based FBG. Results related to Gaussian profile are given in the Appendix.

The FBG structure parameters used in the simulation are chosen to match those of a standard single-mode fiber (SSMF), see Table 1. This is useful to achieve high coupling efficiency at the FBG / SSMF interface. The V-parameter of the FBG is estimated to be 2.24 at  $\lambda=1550$  nm using the expression  $V = \pi d_l \sqrt{n_1^2 - n_2^2} / \lambda$  [32]. Here  $d_l$  is the core diameter,  $n_1$  is the core refractive index, and  $n_2$  is the cladding refractive index. Note that V is lower than 2.405 which is the upper bound for single-mode operation. Unless otherwise stated, the following parameters are used in the simulation: refractive index modulation  $\Delta n = 6 \times 10^{-4}$ , total chirp ( $= \Lambda_{max} - \Lambda_{min} = 2$  nm, and FBG length  $L = 80$  mm.

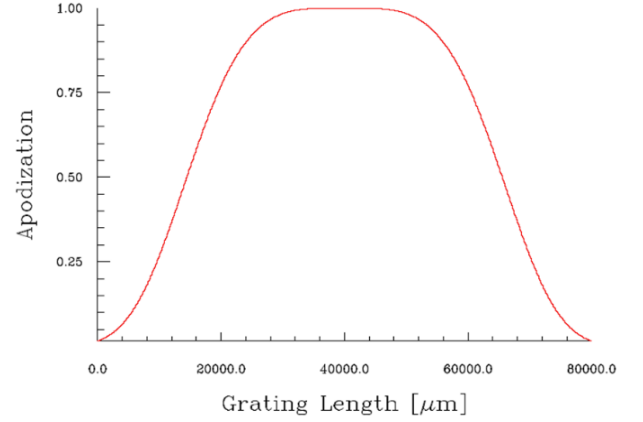
**Table 1.** Parameters values of the LCFBG used in the simulation

Parameter	Value
Core diameter $n_1$	8.5 $\mu\text{m}$
Cladding diameter $n_2$	62.5 $\mu\text{m}$
Core refractive index	1.4600
Cladding refractive index	1.4550
Total chirp	2 nm
Center wavelength	1550 nm
Index modulation	0.0006

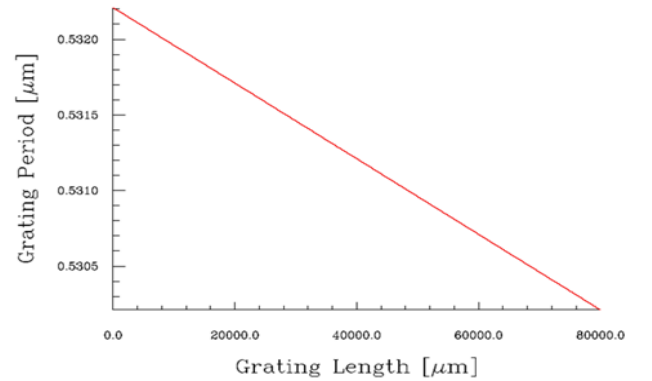
Figure 7 illustrates the main characteristics of a 80 mm-LCFBG designed with MGA ( $n = 4$  and  $s = 0.7$ ). Parts a and b of this figure describe the apodization profile and chirp profile, respectively. The variation of the grating refractive index modulation  $\Delta n(z)$  and grating period  $\Lambda(z)$  along the FBG length is displayed in Figure 7c. Note that the grating period decreases linearly with  $z$  (from  $\Lambda_{max} = 532$  nm at  $z=0$  to  $\Lambda_{min} = 530$  nm at  $z = L$ ). The total chirp is  $\Lambda_{max} - \Lambda_{min} = 2$  nm and the chirp parameter  $C_c = (\Lambda_{max} - \Lambda_{min})/L = 2.5 \times 10^{-2}$  nm/mm. Part d of Figure 7 shows the spectrum of both power reflection and transmission transfer functions. The reflectivity spectrum has a bandwidth  $B_\lambda = 4.07$  nm at -0.5dB level and 0dB peak level at the center wavelength  $\lambda_c = 1550$  nm. The variation of the time delay across the reflectivity spectrum is presented in Figure 7e which shows a linear decrease with wavelength. The maximum time delay difference  $t_d = 562.12$  ps which yields a dispersion parameter  $\beta = 138.11$  ps/nm.

The effect of FBG length on its power reflectivity and time delay spectra is illustrated in Figures 8(a–e) for  $L = 40, 60, 80, 100,$  and  $120$  nm, respectively. The main conclusions drawn from these figures are

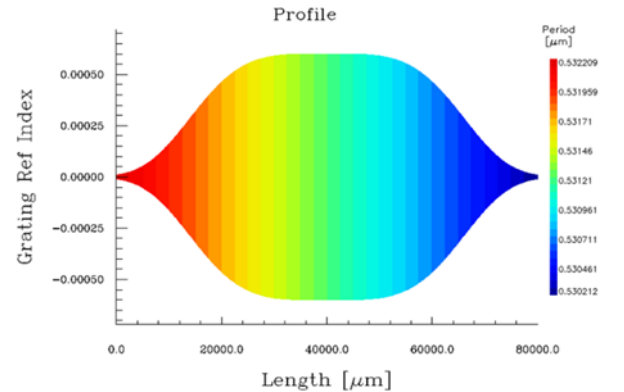
- (i) For  $L = 40, 60,$  and  $80$  mm, the time delay decreases linearly with wavelength and characterized by  $t_d = 251.85, 405.04,$  and  $562.12$  ps over the reflectivity bandwidth  $B_\lambda = 3.65, 3.93$  and  $4.07$  nm respectively. The corresponding dispersion parameters  $\beta$  are  $69, 103.85$  and  $138.11$  ps/nm, respectively.
- (ii) Increasing  $L$  to  $100$  and  $120$  nm destroys the linear  $\tau - \lambda$  characteristics and leads to two and three sections, respectively.



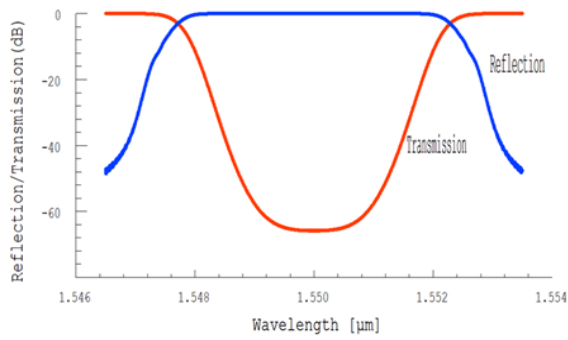
(a)



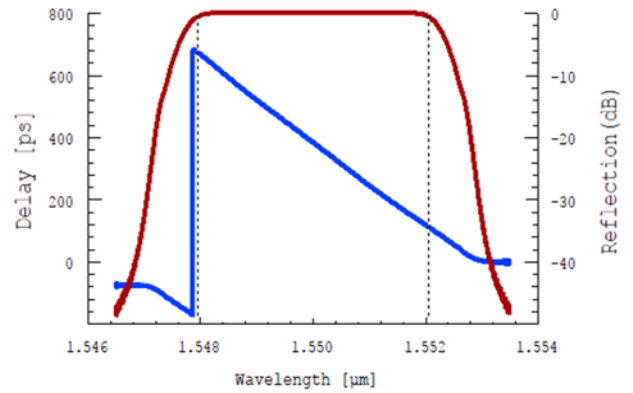
(b)



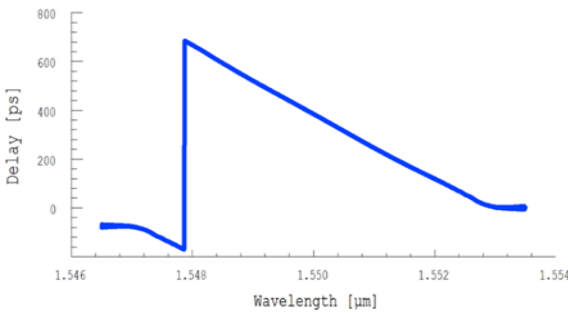
(c)



(d)

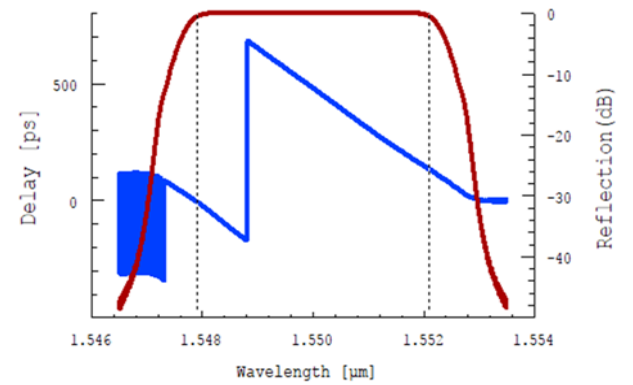


(c)

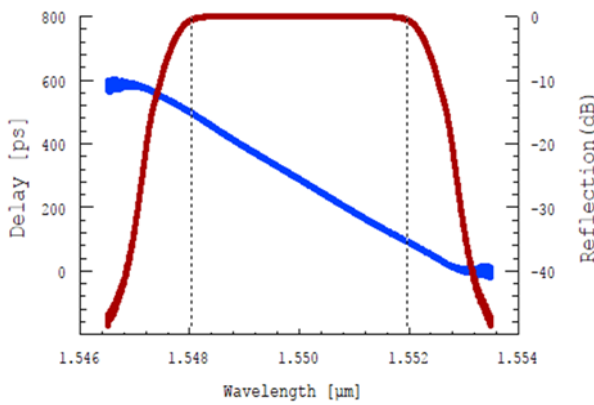


(e)

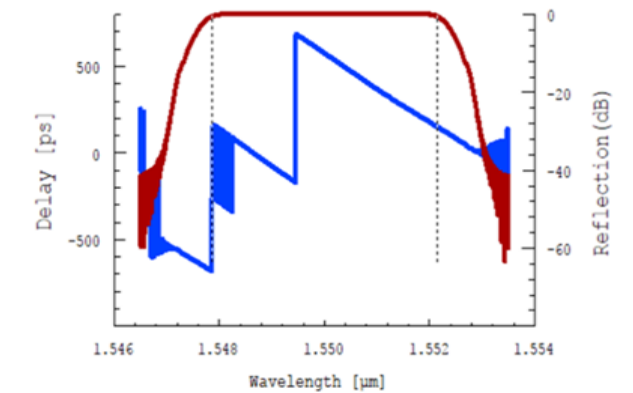
**Figure 7.** Characteristics of 80 mm-LCFBG. (a) Apodization profile (b) Chirp profile. (c) Grating profile. (d) Spectrum of both power reflection and transmission transfer functions. (e) Spectrum of time delay



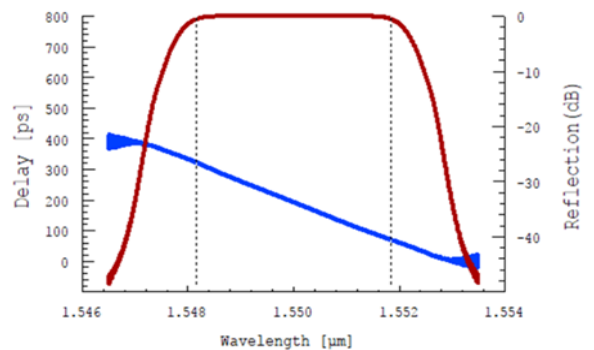
(d)



(a)



(e)



(b)

**Figure 8.** Effect of FBG length on its power reflectivity and time delay spectrum (a) L= 40 mm (b) L= 60 mm (c) L= 80 mm (d) L= 100 mm (e) L= 120 mm. — Delay — Reflection

The dependence of  $B_\lambda$ ,  $t_d$ , and  $\beta$  on FBG length is illustrated in Figures 9(a-c), respectively. At  $L= 95$  nm, the  $t_d-\lambda$  characteristics becomes discontinuous and consists of two linear sections. The discontinuous multisession behavior remains for  $L > 95$  nm. Therefore, the results in Figure 9 are presented for  $L \leq 90$  nm. Note that spectrum bandwidth increases sublinearly with FBG length. In contrast, the parameter  $t_d$  increases almost linearly with  $L$  and reaches a maximum value of 562.12 ps at  $L = 80$  mm. Then  $t_d$

decreases with  $L$  as  $L$  increases toward 90 mm. In the region of  $L \leq 80$  mm, the  $t_d$ - $L$  relation can be fitted by the linear characteristics  $t_d = a + bL$  where  $t_d$  and  $L$  are measured in ps and mm, respectively. Further,  $a = -58.44$  ps and  $b = 7.757$  ps/mm. In other words,  $t_d$  increases by about 7.8 ps for each 1 mm increase in the FBG length when  $L \leq 80$  mm. Note further that the sublinear and linear variations of  $B_\lambda$  and  $t_d$ , respectively, with  $L$  (for  $L \leq 80$  mm region) makes the dispersion parameter  $\beta = t_d/B_\lambda$  an increasing function of  $L$  here. At  $L = 80$  mm,  $t_d$  approaches its maximum value of 562.12ps and  $B_\lambda$  equals 4.07 nm. This leads to  $\beta = 138.11$  ps/nm which represents the maximum dispersion parameter in the region of  $L \leq 80$ mm. Therefore, 80 mm-LCFBGs will be used later to design the beam-steering network. It is worth to mention here that the peak power reflectivity  $R(\lambda_c)$  equals  $-0.71$  dB (85%)  $-0.1$ dB (98%), and 0dB (100%) at  $L=10, 20,$  and  $\geq 30$  mm, respectively.

The simulation is extended further to investigate the effect of total chirp on the characteristic of the 80 mm-LCFBG and the results are presented in Figure 10. The performance parameters are recorded when the total chirp is varied from 1.8 to 2.3 nm. The main conclusions drawn for this figure are

- (i) The bandwidth  $B_\lambda$  increases linearly with the total chirp (slope = 1.74).
- (ii) The time delay difference  $\tau_d$  decreases slightly and almost linearly with the total chirp (slope  $\cong -50$  ps/nm).
- (iii) The dispersion parameter decreases almost linearly with total chirp (slope  $\approx -71$  ps/nm).

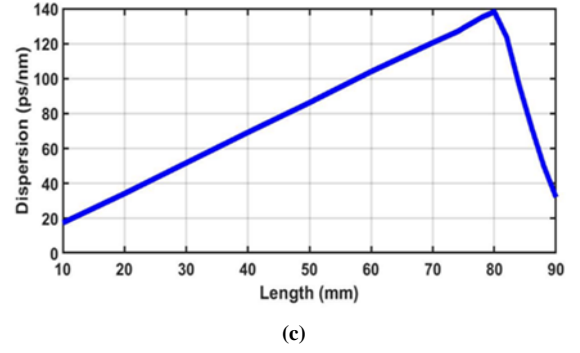
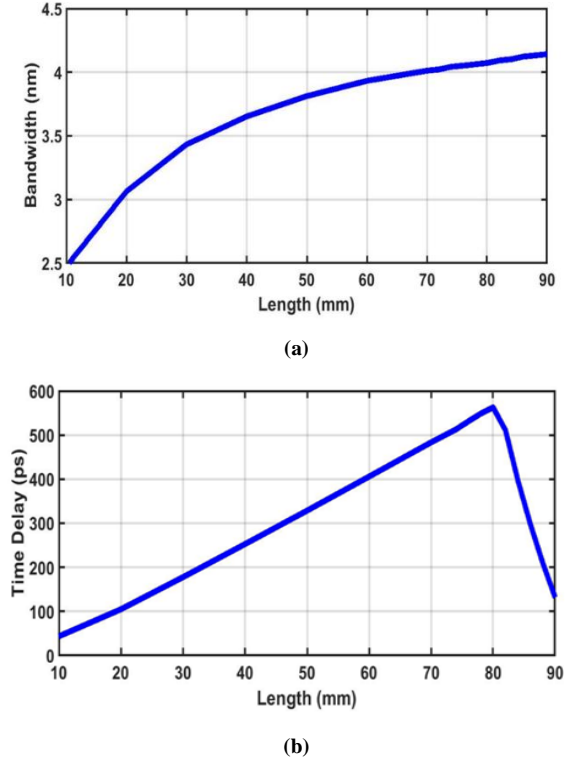


**Figure 9.** Effect of FBG length on the (a) bandwidth (b) time delay (c) dispersion

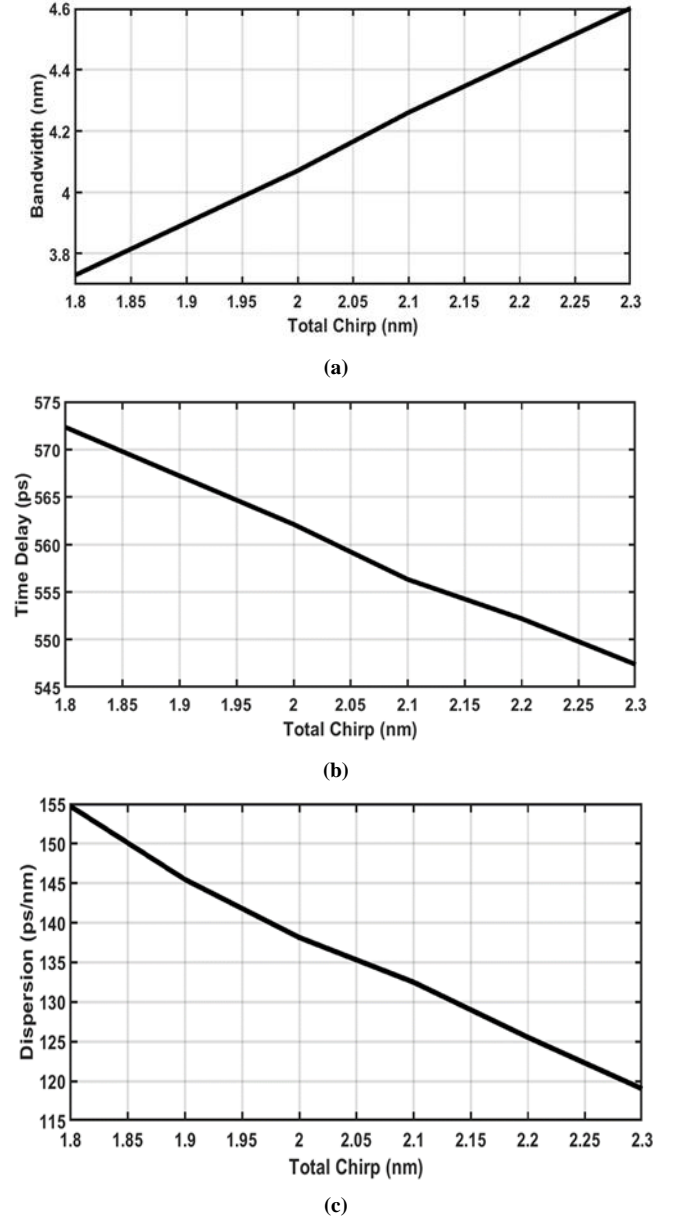


**Figure 10.** Effective of total chirp of 80 mm-LFBG on the (a) bandwidth. (b) time delay. (c) dispersion

According to the above conclusions, the following question needs to be answered. Which is the suitable value of

the total chirp that can be used to design the LCFBG for the beam-steering network?. Using FBG with large bandwidth makes its suitable for use with large N-PAA. Further, FBG with large time delay difference reduces the lower bound of the microwave frequency to be steered. In this work, a total chirp of 2 nm is used as a trade off between the two mentioned performance parameters,  $\lambda_B$  and  $t_d$ .

Table 2 lists performance comparison between two LCFBGs, one is designed with MGA ( $n = 4$  and  $s = 0.7$ ) and the other is designed with GA ( $s = 0.5$ ). The comparison results are presented for three FBG lengths (40, 60 and 80 mm). Other structure parameters used in the simulation are identical for both FBGs as given in Table 1. The simulation reveals that the peak power reflectivity is 0dB for all the cases considered here and therefore not listed in Table 2. Investigation the results in Table 2 highlights the following findings. Using MGA enhances both spectrum bandwidth  $B_\lambda$  and time delay  $t_d$  almost by the same factor over GA. This leads to approximately the same dispersion parameter  $\beta$  for the two apodization profiles. This enhancement factor is about 1.30, 1.22, and 1.18 for L= 40, 60, and 80 mm, respectively. From engineering point of view, one can say that MGA offers about 20-30% increase in both  $B_\lambda$  and  $t_d$  over GA and this leads to the same dispersion parameter  $\beta$ .

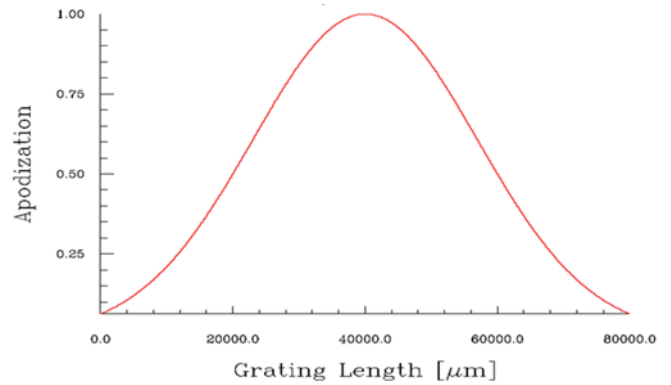
**Table 2.** Performance comparison between MGA- and MA-LCFBGs

FBG Length (mm)	Apodization profile	Reflection spectrum bandwidth (nm)	Maximum time delay difference $t_d$ (ps)	Dispersion parameter (ps/nm)
40	Modified Gaussian	3.65	251.85	69.00
	Gaussian	2.81	192.66	68.56
60	Modified Gaussian	3.90	405.04	103.85
	Gaussian	3.19	331.13	103.80
80	Modified Gaussian	4.07	562.12	138.11
	Gaussian	3.45	478.15	138.59

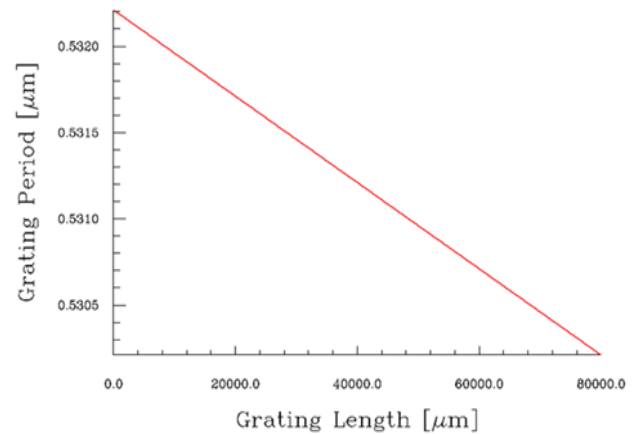
## 5. Conclusions

A Configurable photonic true time delay line (TTDL) consisting of cascaded linearly chirped fiber Bragg grating (LCFBGs) has been proposed to support the design of PAA beam-steering networks. Parametric study of the designed LCFBG has been performed and the simulation results reveal that designing the LCFBG with modified Gaussian apodization (MGA) offers high-performance time delay characteristics. A LCFBG of 80mm length offers 562.12 ps time delay difference across the 4.07 nm spectrum spectral bandwidth. The length of the LCFBG should be chosen carefully to yield a linear time delay-optical wavelength characteristics. Designing the LCFBG with  $L > 80$  mm will destroys this linear relation.

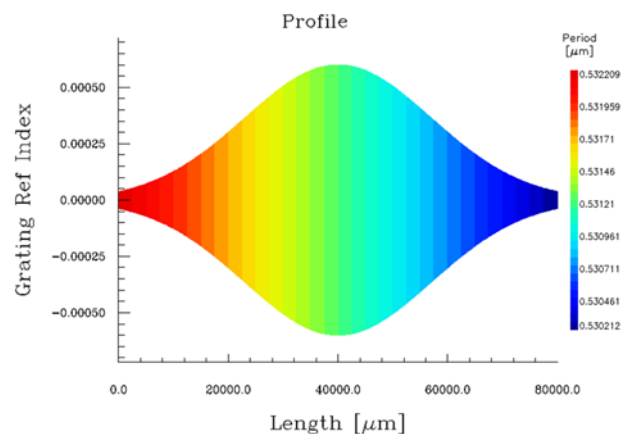
## Appendix Performance Parameters of LCFBG Design with Gaussian Apodization



(a)

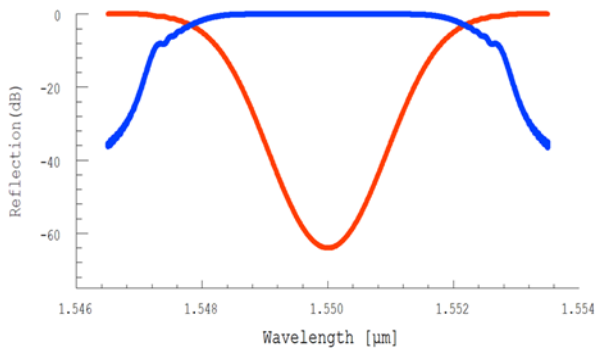


(b)



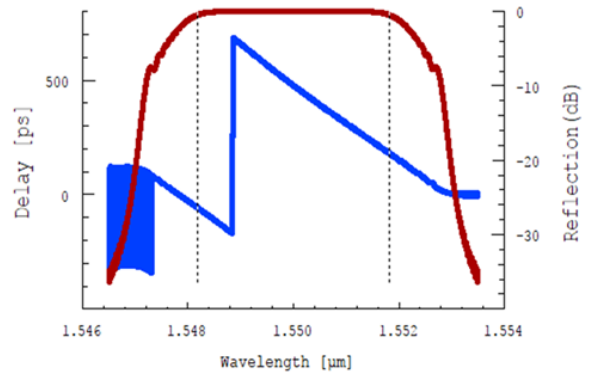
(c)

**Figure A1.** Characteristics of 80 mm-LCFBG. (a) Apodization profile. (b) Chirp profile. (c) Grating profile. (d) Spectrum of both power reflection and transmission transfer functions

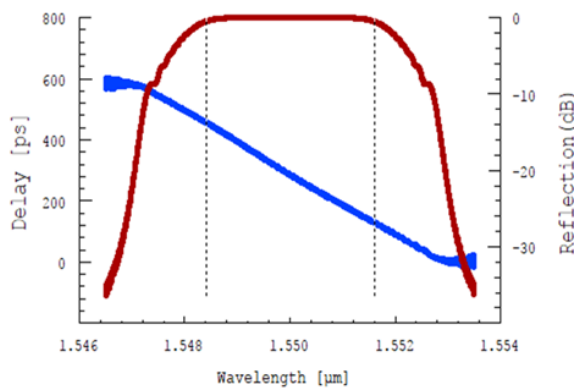


(d)

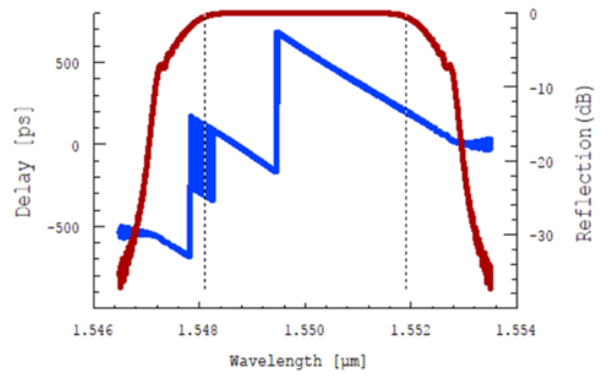
Figure A1. (Continued)



(d)

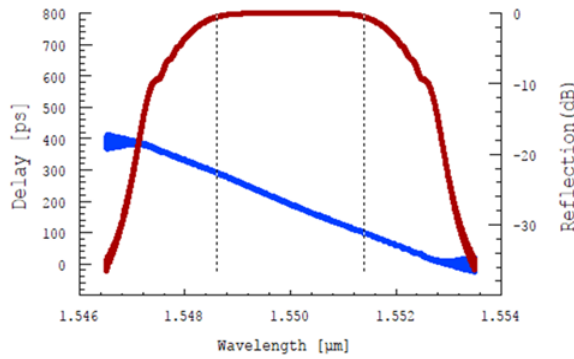


(a)

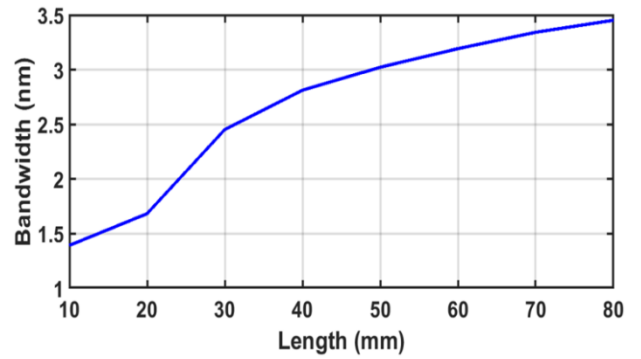


(e)

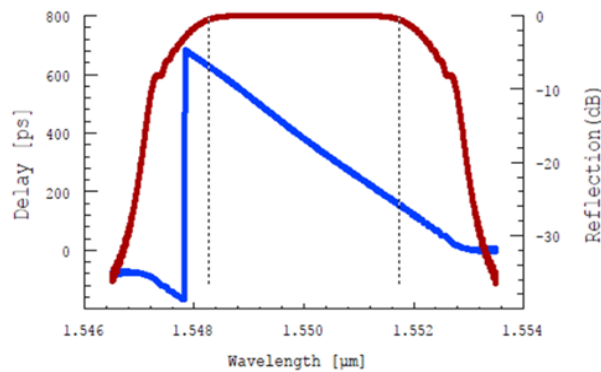
Figure A2. Effect of FBG length on its power reflectivity and time delay spectra (a) L= 40 mm (b) L= 60 mm (c) L= 80 mm (d) L= 100 mm (e) L= 120 mm. — Delay — Reflection



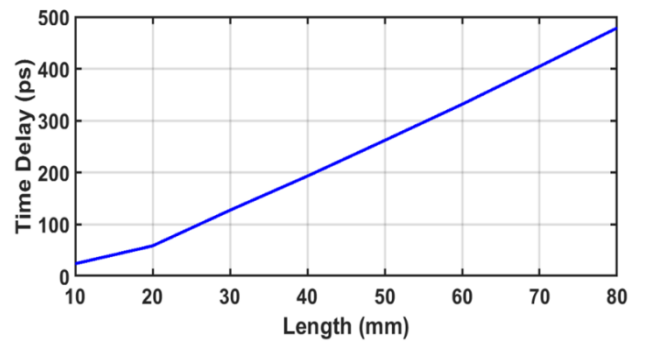
(b)



(a)



(c)



(b)

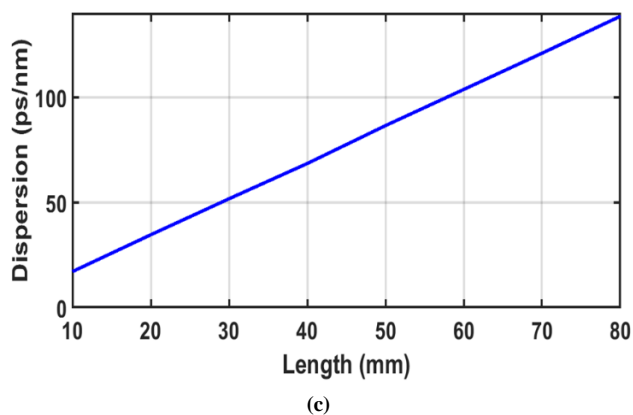


**Figure A3.** Effect of FBG Length on the (a) bandwidth (b) time delay and (c) dispersion

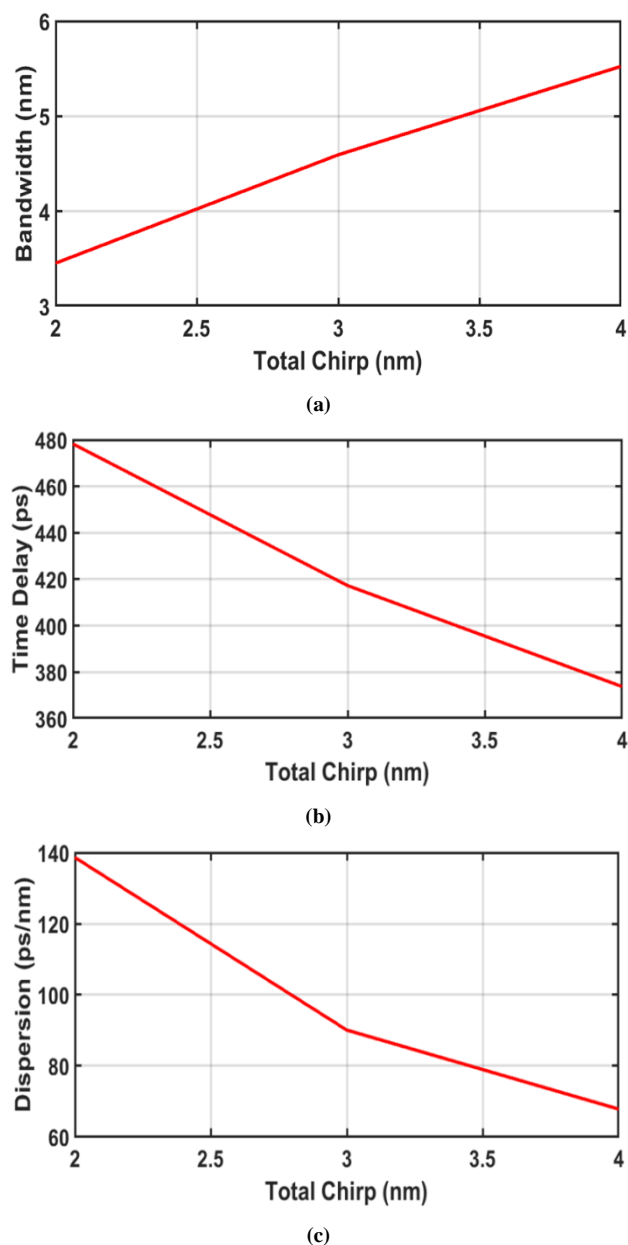


**Figure A4.** Effectiveness of total chirp of 80 mm-LFBG on the (a) bandwidth (b) time delay and (c) dispersion

## REFERENCES

- [1] D. A. K. Aljaf, R. S. Fyath, "Configurable Beam-Steering Network for Phase Array Antennas- Part II: Design Guidelines and Results", Submitted to International Journal of Networks and Communications, 2019.
- [2] D. Perez, I. Gasulla, and Jose Capmany, "Toward Programmable Microwave Photonics Processors", IEEE Journal of Lightwave Technology, vol. 36, no. 2, pp. 519-532, Jan. 2018.
- [3] T. Li, E. H. W. Chan, X. Wang, X. Feng, B. Guan, J. Yao, "Broadband Photonic Microwave Signal Processor With Frequency Up/Down Conversion and Phase Shifting Capability", IEEE Photonics Journal, vol. 10, no. 1, Article no. 5500112, pp. 1-13, Feb. 2018.
- [4] R. Bonjour, M. Singleton, S. A. Gebrewold, Y. Salamin, F. C. Abrecht, B. Baeuerle, A. Josten, P. Leuchtman, C. Hafner, and J. Leuthold, "Ultra-Fast Millimeter Wave Beam-Steering", IEEE Journal of Quantum Electronics, vol. 52, no. 1, Article no. 0600708, pp. 1-8, Jan. 2016.
- [5] L.E. Y. Herrera, R. M. Ribeiro, V. B. Jabulka, P. Tovar, and J. P. Weid, "Photonic Generation and Transmission of Linearly Chirped Microwave Pulses With High TBWP by Self-Heterodyne Technique", IEEE Journal of Lightwave Technology, vol. 36, no. 19, pp. 4408-4415, Oct. 2018.
- [6] L. R. Chen, "Silicon Photonics for Microwave Photonics Applications", IEEE Journal Photonic Technology Letters, vol. 35, no. 4, pp. 824- 835, Feb. 2017.
- [7] Y. Zhang, and Sh. Pan, "Broadband Microwave Signal Processing Enabled by Polarization-Based Photonic Microwave Phase Shifters", IEEE Journal of Quantum Electronics, vol. 54, no. 4, Article no. 0700112, pp. 1-12, Aug. 2018.
- [8] L. Huo, L. Gan , L. Shen, M. Tang, S. Fu, C. Yang, and W. Tong, "IIR Microwave Photonic Filters Based on Homogeneous Multicore Fibers", IEEE Journal of Lightwave Technology, vol. 36, no. 19, pp. 4298- 4304, Oct. 2018.
- [9] S. Song, S. X. Chew, X. Yi, L. Nguyen, and R. A. Minasian, "Tunable Single Passband Microwave Photonic Filter Based on Integrated Optical Double Notch Filter", IEEE Journal of Lightwave Technology, vol. 36, no. 19, pp. 4557- 4564, Oct. 2018.
- [10] R. Bonjour, M. Singleton, S. A. Gebrewold, Y. Salamin, F. C. Abrecht, B.Baeuerle, A. Josten, P. Leuchtman, C. Hafner, and J. Leuthold, "Ultra-Fast Millimeter Wave Beam-Steering", IEEE Journal of Quantum Electronics, vol. 52, no. 1, Article no. 0600708, pp. 1-8, Jan. 2016.
- [11] Z. Cao, Q. Ma, A. B. Smolders, Y. Jiao, M. J. Wale, Ch. W. Oh, H. Wu, and A. M. J. Koonen, "Advanced Integration Techniques on Broadband Millimeter-Wave Beam-Steering for 5G Wireless Networks and Beyond", IEEE Journal of Quantum Electronics, vol. 52, no. 1, Article no. 0600620, pp. 1-20, Jan. 2016.
- [12] M. Imbert , J. Romeu, M. B. Escudero, M.T. M. Ingles, J. M. M. G. Pardo, and L. Jofre, "Assessment of LTCC-Based

- Dielectric Flat Lens Antennas and Switched-Beam Arrays for Future 5G Millimeter-Wave Communication Systems", *IEEE Transaction On Antenna and Propagation*, vol. 65, no. 12, pp. 6453-6473 Dec. 2017.
- [13] G. Serafino, C. Porzi, F. Falconi, S. Pinna, M. Puleri, A. D. Errico, A. Bogoni, and P. Ghelfi, "Photonics-Assisted Beam-forming for 5G Communications", *IEEE Journal Photonic Technology Letters*, vol. 30, no. 21, pp. 1826- 1829, Nov. 2018.
- [14] Z. G. Tegegne, C. Decroze, Ph. D. Bin, T. Fromenteze, and C. Aupetit-Berthelemot, "Single Channel Microwave Photonics Digital Beamforming Radar Imaging System", *IEEE Journal Photonic Technology Letters*, vol. 36, no. 3, pp. 675- 681, Feb. 2018.
- [15] J. F. Diehl, J. M. Singley, C. E. Sunderman, and V. J. Urick, "Microwave photonic delay line signal processing", *Applied Optics*, vol. 54, no. 31, pp F35-F41, Nov. 2015.
- [16] X. Ye, D. Zhu, Y. Zhang, S. Li, and S. Pan, "Analysis of Photonics-Based RF Beamforming With Large Instantaneous Bandwidth", *IEEE Journal of Lightwave Technology*, vol. 35, no. 23, pp. 5010- 5019, Dec. 2017.
- [17] R. J. Mailloux, "Phased Array Antenna Handbook", 3<sup>rd</sup> Ed., Artech House 2018.
- [18] R. Kashyab, "Fiber Bragg Gratings", Suite 400, 2<sup>nd</sup> Ed., 2010.
- [19] D. Tosi, "Review of Chirped Fiber Bragg Grating (CFBG) Fiber-Optic Sensors and Their Applications", *Sensors*, vol. 18, Article no. 2147, pp. 1-32, Jul. 2018.
- [20] S. B. A. Ghatak, "Guided Wave Optics and Photonic Devices", Taylor and Francis Group, 2013.
- [21] S. Khan, and S. Fathpour, "Demonstration of Tunable Optical Delay Lines Based on Apodized Grating Waveguides", *Optics Express*, vol. 21, no. 17, pp. 19538-19543, Aug. 2013.
- [22] G. Palumbo, D. Tosi, A. Iadicicco, S. Campopiano, "Analysis and Design of Chirped Fiber Bragg Grating for Temperature Sensing for Possible Biomedical Applications", *IEEE Photonics Journal*, vol. 10, no. 3, Article no. 7103015, pp. 1-16, Jun, 2018.
- [23] H. Zwickel, S. Wolf, C. Kieninger, Y. K. Vida, M. Lauermann, T. D. Keulenaer, A. Vyncke, R. Vaernewyck, J. Luo, A. K. Y. Jen, W. Freude, J. Bauwelinck, S. Randel, and C. Koos, "Silicon-Organic Hybrid (SOH) Modulators for Intensity-Modulation / Direct-Detection Links With Line Rates of Up to 120 Gbit/s", *Optics Express*, vol. 25, no. 20, pp. 23784-23800, Oct. 2017.
- [24] T. Sato, T. Fujisawa, K. Saitoh, "All-Optical Diode Suppressing Broadband Backward Transmission Using Single- and Four-Port Photonic Crystal Cavities", *IEEE Photonics Journal*, vol. 11, no. 1, Article no. 4900214, pp. 1-15, Feb. 2018.